

# Interspecies thermalization in an ultracold mixture of Cs and Yb in an optical trap

A. Guttridge,<sup>1,\*</sup> S. A. Hopkins,<sup>1</sup> S. L. Kemp,<sup>1</sup> Matthew D. Frye,<sup>2,†</sup> Jeremy M. Hutson,<sup>2</sup> and Simon L. Cornish<sup>1,‡</sup>

<sup>1</sup>*Joint Quantum Centre (JQC) Durham-Newcastle, Department of Physics, Durham University, South Road, Durham, DH1 3LE, United Kingdom.*

<sup>2</sup>*Joint Quantum Centre (JQC) Durham-Newcastle, Department of Chemistry, Durham University, South Road, Durham, DH1 3LE, United Kingdom.*

(Dated: October 27, 2021)

We present measurements of interspecies thermalization between ultracold samples of  $^{133}\text{Cs}$  and either  $^{174}\text{Yb}$  or  $^{170}\text{Yb}$ . The two species are trapped in a far-off-resonance optical dipole trap and  $^{133}\text{Cs}$  is sympathetically cooled by Yb. We extract effective interspecies thermalization cross sections by fitting the thermalization measurements to a kinetic model, giving  $\sigma_{\text{Cs}^{174}\text{Yb}} = (5 \pm 2) \times 10^{-13} \text{ cm}^2$  and  $\sigma_{\text{Cs}^{170}\text{Yb}} = (18 \pm 8) \times 10^{-13} \text{ cm}^2$ . We perform quantum scattering calculations of the thermalization cross sections and optimize the CsYb interaction potential to reproduce the measurements. We predict scattering lengths for all isotopic combinations of Cs and Yb. We also demonstrate the independent production of  $^{174}\text{Yb}$  and  $^{133}\text{Cs}$  Bose-Einstein condensates using the same optical dipole trap, an important step towards the realization of a quantum-degenerate mixture of the two species.

The realization of ultracold atomic mixtures [1–12] has opened up the possibility of exploring new regimes of few- and many-body physics. Such mixtures have been used to study Efimov physics [13–15], probe impurities in Bose gases [16], and entropically cool gases confined in an optical lattice [17]. Pairs of atoms in the mixtures can be combined using magnetically or optically tunable Feshbach resonances to create ultracold molecules [18–26]. These ultracold molecules have a wealth of applications, such as tests of fundamental physics [27–29], realization of novel phase transitions [30–32], and the study of ultracold chemistry [33, 34]. In addition, the long-range dipole-dipole interactions present between pairs of polar molecules make them useful in the study of dipolar quantum matter [35, 36] and ultracold molecules confined in an optical lattice can simulate a variety of condensed-matter systems [37–39].

Although the large majority of work on ultracold molecules has focused on bi-alkali systems, there is burgeoning interest in pairing alkali-metal atoms with divalent atoms such as Yb [40–45] or Sr [46]. The heteronuclear  $^2\Sigma$  molecules formed in these systems have both an electric and a magnetic dipole moment in the ground electronic state. The extra magnetic degree of freedom opens up new possibilities for simulating a range of Hamiltonians for spins interacting on a lattice and for topologically protected quantum information processing [47].

One of the challenging aspects of creating molecules in these systems is that the Feshbach resonances tend to be narrow and sparse. They are narrow because the main coupling responsible for them is the weak distance dependence of the alkali-metal hyperfine coupling, caused by the spin-singlet atom at short range [48]. They are sparse because only molecular states with the same value of the alkali-metal magnetic quantum number  $M_F$

as the incoming atomic channel can cause resonances. The resonance positions are determined by the (often unknown) background scattering length [48, 49], and for some systems may be at impractically high magnetic fields. Amongst the various alkali-Yb combinations, CsYb has been proposed as the most favorable candidate because the high mass of Cs facilitates a higher density of bound states near threshold and its large hyperfine coupling constant increases the resonance widths [49]. However, the short-range part of the molecular ground-state potential is not known accurately enough to predict background scattering lengths, so experimental characterization is essential before accurate predictions of resonance positions and widths can be made.

Here we present simultaneous optical trapping of Cs and Yb and first measurements of the scattering properties of  $^{133}\text{Cs}+^{174}\text{Yb}$  and  $^{133}\text{Cs}+^{170}\text{Yb}$ . We measure interspecies thermalization in the optical dipole trap and use a kinetic model to extract effective thermalization cross sections. We model these cross sections using quantum scattering calculations, taking full account of the anisotropy of differential cross sections and thermal averaging. We obtain an optimized interaction potential and use it to make predictions of the scattering lengths for all accessible isotopologs. For all isotopes except  $^{176}\text{Yb}$ , binary quantum-degenerate mixtures of Cs and Yb are expected to be miscible at fields around 22 G, where the Efimov minimum in the three-body recombination rate allows efficient evaporation of Cs to quantum degeneracy [50].

## I. EXPERIMENT

A detailed description of our experimental apparatus can be found in [51], but we will summarize the main components here. Cs and Yb magneto-optical traps (MOTs) are sequentially loaded from an atomic beam that effuses from a dual-species oven and is slowed by a dual-species Zeeman slower [52]. The Cs atomic beam is

\* alexander.guttridge@durham.ac.uk

† matthew.frye@durham.ac.uk

‡ s.l.cornish@durham.ac.uk

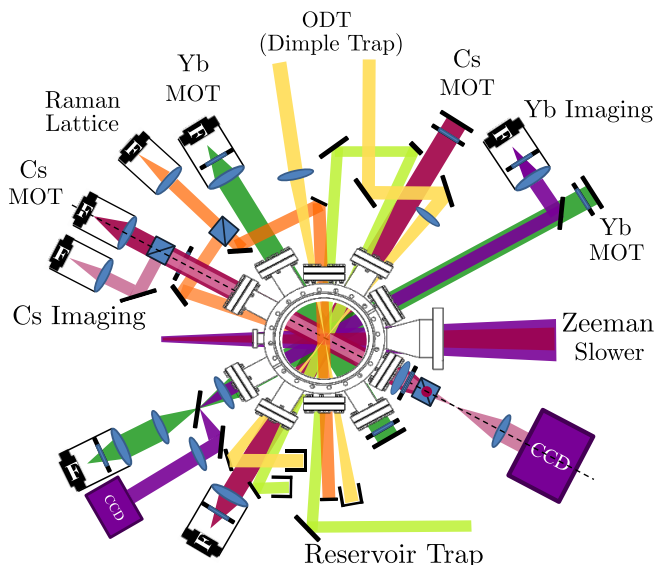


FIG. 1. Optical layout of the science chamber in the horizontal plane. The Cs (Yb) imaging beam is combined with the Cs (Yb) MOT beam using a polarizing beam splitter (dichroic mirror) and then separated after the chamber and aligned onto a CCD camera. The Raman lattice beams used for DRSC are split using a polarizing beam splitter, with one arm retro-reflected and the other arm dumped after the first pass. The ODT used for thermalization measurements is referred to as the “dimple trap” to distinguish it from the large-volume “reservoir trap” that is used for the preparation of Cs BEC.

slowed and trapped in the MOT using the  $^2S_{1/2} \rightarrow ^2P_{3/2}$  transition at  $\lambda = 852$  nm. For Yb we use the broad  $^1S_0 \rightarrow ^1P_1$  transition at  $\lambda = 399$  nm ( $\Gamma/2\pi = 29$  MHz) for Zeeman slowing and absorption imaging, and the narrow  $^1S_0 \rightarrow ^3P_1$  transition at  $\lambda = 556$  nm ( $\Gamma/2\pi = 182$  kHz) for laser cooling in the MOT. The optical layout of our science chamber is shown in Fig. 1.

The thermalization measurements presented here take place in an optical dipole trap (ODT) formed from the output of a broadband fiber laser (IPG YLR-100-LP) with a wavelength of  $1070 \pm 3$  nm. The ODT consists of two beams crossed at an angle of  $40^\circ$  with waists of  $33 \pm 3$   $\mu\text{m}$  and  $72 \pm 4$   $\mu\text{m}$  respectively. The intensity of each beam is independently controlled by a water-cooled acousto-optic modulator. Yb has a moderately low polarizability at the trapping wavelength ( $\alpha_{\text{Yb}}(1070 \text{ nm}) = 150 a_0^3$ ) so that, for the powers used in the thermalization measurements, Yb atoms are trapped only in the part of the potential where the axial confinement is provided by the second ODT beam. Cs, on the other hand, has a much larger polarizability at the trapping wavelength ( $\alpha_{\text{Cs}}(1070 \text{ nm}) = 1140 a_0^3$ ), creating a trap deep enough that Cs atoms are confined both inside and outside the crossed-beam region of the ODT. Some Cs atoms thus experience a trapping potential dominated by just a single ODT beam.

A summary of the experimental sequence used for the

thermalization measurements is shown in Fig. 2. The two species are sequentially loaded into the dipole trap to avoid unfavorable inelastic losses from overlapping MOTs [53]. We choose to prepare the Yb first due to the much longer loading time of the MOT and its insensitivity to magnetic fields. We first load the Yb MOT for 10 s, preparing  $5 \times 10^8$  atoms at  $T = 140$   $\mu\text{K}$  [54], before ramping the power and detuning the MOT beams to cool the atoms to  $T = 40$   $\mu\text{K}$ . We load  $1.8 \times 10^7$  atoms into the ODT with a trap depth of  $U_{\text{Yb}} = 950$   $\mu\text{K}$ . We then evaporatively cool the atoms by exponentially reducing the trap depth to  $U_{\text{Yb}} = 5$   $\mu\text{K}$  in 7 s, producing a sample of  $1 \times 10^6$  Yb atoms at a temperature of  $T = 550$  nK. At this stage the Yb trap frequencies as measured by center-of-mass oscillations are 240 Hz radially and 40 Hz axially.

Once the Yb is prepared in the dipole trap, the Cs MOT is loaded for 0.15 s, at which point the MOT contains  $1 \times 10^7$  atoms. The Cs MOT is then compressed via ramps to the magnetic field, laser intensity and detuning before it is overlapped with the ODT using magnetic bias coils. The Cs atoms are then further cooled by optical molasses before transfer into a near-detuned lattice with  $P = 100$  mW, where the atoms are then polarized in the  $|F = 3, m_F = +3\rangle$  state and cooled to  $T = 2$   $\mu\text{K}$  with 8 ms of degenerate Raman sideband cooling (DRSC). During this stage  $9 \times 10^4$  atoms are transferred into the ODT and the magnetic bias field is set to 22.3 G, corresponding to the Efimov minimum in the Cs three-body recombination rate [50]. During the transfer the atoms are heated to  $T = 5$   $\mu\text{K}$ . The heating and poor efficiency of the transfer into the ODT are due to the poor mode matching of the DRSC-cooled cloud and the deep ODT ( $U_{\text{Cs}} = 85$   $\mu\text{K}$ ). This huge ratio of trap depths  $U_{\text{Cs}}/U_{\text{Yb}} = 15.5$  is greater than the (still large) ratio of the polarizabilities  $\alpha_{\text{Cs}}/\alpha_{\text{Yb}} = 7.2$  due to the effect of gravity on the weak Yb trap. The ratio of the mean trap frequencies between the two species is  $\bar{\omega}_{\text{Cs}}/\bar{\omega}_{\text{Yb}} = 3.1$ .

The thermalization measurements thus begin with a mixture of  $1 \times 10^6$  Yb atoms in their spin-singlet ground state  $^1S_0$  and  $9 \times 10^4$  Cs atoms in their absolute ground state  $^2S_{1/2} |3, +3\rangle$ . For each experimental run the number and temperature are determined by quickly turning off the ODT after a variable hold time and performing resonant absorption imaging of both species after a variable time of flight.

Figure 3 shows the number and temperature evolution of Cs and  $^{174}\text{Yb}$  atoms, with and without the other species present. The smaller initial number of Cs atoms is chosen to reduce the density of Cs such that the effects of three-body recombination play a relatively small role in the thermalization [55]. Treatment of the number evolution of the Cs atoms requires careful attention due to the presence of Cs atoms both in the crossed-beam region of the trap and in the wings, where confinement is due to only a single ODT beam. Although the Cs atoms in the crossed- and single-beam regions are in thermal equilibrium, the atoms have different density distributions

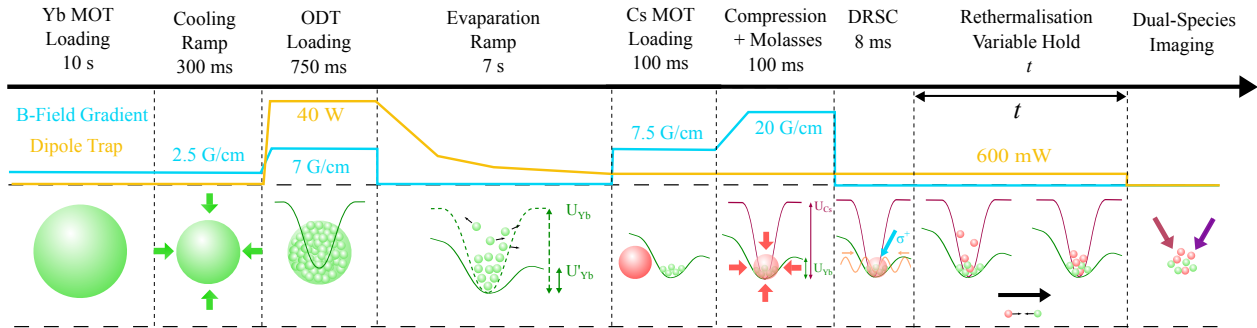


FIG. 2. Simplified experimental sequence. The Yb MOT is loaded, then cooled and compressed to facilitate subsequent loading into an ODT. The Yb is then evaporated in the ODT by ramping the trap depth until a temperature of  $T = 550$  nK is reached. The displaced Cs MOT is loaded before it is compressed, cooled and transferred into a near-detuned optical lattice for DRSC. The DRSC stage loads Cs into the ODT, where it is held with Yb for a variable time  $t$  before the trap is switched off and the atoms are destructively imaged after a variable time of flight using dual-species absorption imaging.

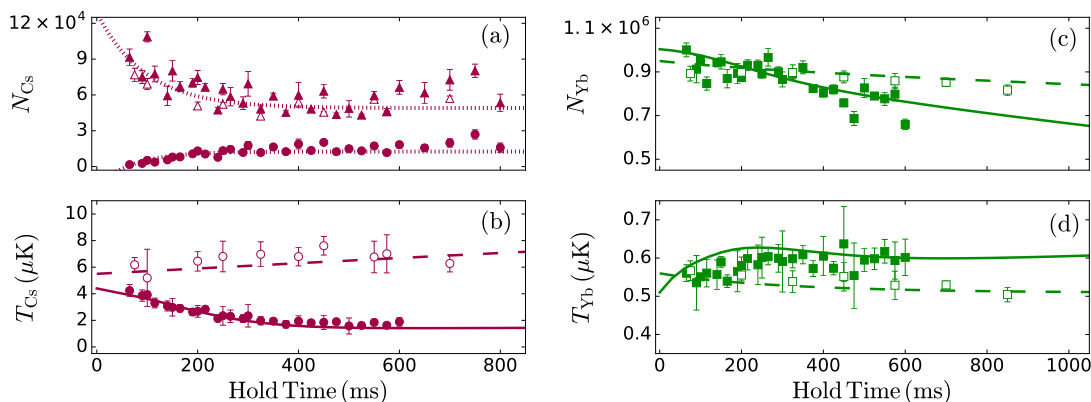


FIG. 3. Results of thermalization experiments. (a) and (b) show the evolution of the Cs number and temperature as a function of hold time  $t$ . (c) and (d) show the  $^{174}\text{Yb}$  number and temperature as a function of the same hold time. Filled symbols indicate the presence of both Cs and  $^{174}\text{Yb}$  in the ODT, whereas open symbols indicate the presence of only one species in the trap. For the Cs number, triangles indicate the number in the single-beam region of the trap and circles the number in the crossed-beam region, while dotted lines show the interpolating functions used to constrain the Cs number in the model. The dashed line shows the result of our kinetic model with only one species trapped and the solid line shows the result for the two-component mixture.

due to the different potentials experienced. This is an important effect to consider when calculating the spatial overlap of the Cs and Yb atoms. We observe an increase in the number of Cs atoms trapped in the crossed-beam region of the trap in the presence of Yb, which we attribute to interspecies collisions aiding the loading of this region. We do not observe any Cs atoms loaded into the crossed-beam portion of the trap in the absence of Yb, so the number is not plotted in this case. For the Cs atoms in the single-beam region, we estimate the axial trapping frequency to be the same as for a single-beam trap, 5 Hz, and the radial frequencies to be the same as in the crossed-beam region.

We observe a decay of the Yb number throughout the thermalization. The timescale of this decay is much

shorter than the single-species  $1/e$  background lifetime of 15 s and we attribute the number loss to sympathetic evaporation [2]. The small change in the Yb temperature is explained in part by the evaporation of hotter atoms and also by the large number ratio  $N_{Yb}/N_{Cs}$ , which causes the final mean temperature of the sample to be close to the initial Yb temperature. In contrast to Yb, we observe a large change in the temperature of the Cs atoms for short times due to elastic collisions with the Yb atoms. However, for longer times we see the two species reach a steady state at two distinct temperatures. The higher final temperature for Cs results from a Cs heating rate that balances the sympathetic cooling rate.

## II. RATE EQUATIONS FOR THERMALIZATION

To model the thermalization results, we formulate a set of coupled equations that describe the number and

$$\dot{N}_i = -N_i \gamma_{ii} \eta_i \exp(-\eta_i) - K_{\text{bg}} N_i - K_{i,3} \langle n_i^2 \rangle_{\text{sp}} N_i, \quad (1)$$

$$\dot{T}_i = \eta_i \exp(-\eta_i) \gamma_{ii} \left(1 - \frac{\eta_i + \kappa_i}{3}\right) T_i + K_{i,3} \langle n_i^2 \rangle_{\text{sp}} \frac{(T_i + T_{i,\text{H}})}{3} \pm \frac{\xi \Gamma_{\text{CsYb}} \Delta T(t)}{3N_i} + \dot{T}_{i,\text{ODT}}, \quad (2)$$

where  $i = \{\text{Yb}, \text{Cs}\}$ ,  $\eta_i = U_i/k_{\text{B}}T_i$ , and  $\kappa_i = (\eta_i - 5)/(\eta_i - 4)$  [60].  $K_{\text{bg}}$  is the background loss rate,  $K_{i,3}$  is the three-body loss coefficient,  $n_i(\mathbf{r})$  is the density and  $\langle \dots \rangle_{\text{sp}}$  represents a spatial average.  $T_{i,\text{H}}$  is the recombination heating term, which accounts for the increase in temperature due to the release of the molecular binding energy during recombination [59]. We choose to neglect the three-body loss coefficient for Yb,  $K_{\text{Yb},3}$ , because we do not observe any evidence of three-body loss on the experimental timescale in single-species Yb experiments. The Cs three-body loss coefficient is measured to be  $K_{\text{Cs},3} = 1_{-0.9}^{+1} \times 10^{-26} \text{ cm}^6/\text{s}$  at the bias field used in the measurements. In addition to the above terms,  $\dot{T}_{i,\text{ODT}}$  is added as an independent heating term to account for any heating from the trapping potential, such as off-resonant photon scattering [61] or additional heating effects due to the multi-mode nature of the trapping laser [62–65]. The heating rate for Yb alone is found to

temperature kinetics. We expand upon the usual treatment [41, 42, 56, 57] by including terms for evaporation [58] and single-species three-body recombination [59] as described in the Appendix. The coupled equations for the number  $N_i$  and temperature  $T_i$  of the two species are

be zero within experimental error, so  $\dot{T}_{\text{Yb},\text{ODT}}$  is fixed at 1 nK/s, which is the predicted heating rate due to off-resonant photon scattering. Eq. 2 uses the fact that the average energy transferred in a hard-sphere collision is  $\xi k_{\text{B}} \Delta T$ , where  $\xi = 4m_{\text{Cs}}m_{\text{Yb}}/(m_{\text{Cs}} + m_{\text{Yb}})^2$ ,  $m_i$  is the mass of species  $i$ , and  $\Delta T = T_{\text{Cs}} - T_{\text{Yb}}$ .

The effective intraspecies collision rate per atom for thermalization is  $\gamma_{ii} = \langle n_i \rangle_{\text{sp}} \sigma_{ii} \bar{v}_{ii}$ , where  $\sigma_{ii}$  is an effective energy-independent scattering cross section. In a hard-sphere model, the effective total interspecies collision rate is  $\Gamma_{\text{CsYb}} = \bar{n}_{\text{CsYb}} \sigma_{\text{CsYb}} \bar{v}_{\text{CsYb}}$ , where the mean thermal velocity  $\bar{v}_{ij}$  is

$$\bar{v}_{ij} = \sqrt{\frac{8k_{\text{B}}}{\pi} \left( \frac{T_i}{m_i} + \frac{T_j}{m_j} \right)} \quad (3)$$

and the spatial overlap  $\bar{n}_{\text{CsYb}}$  is found by integrating the density distributions of the two species,

$$\begin{aligned} \bar{n}_{\text{CsYb}} &= \int [n_{\text{Cs},\text{single}}(\mathbf{r}) + n_{\text{Cs},\text{cross}}(\mathbf{r})] n_{\text{Yb}}(\mathbf{r}) d^3r \\ &= N_{\text{Yb}} \frac{m_{\text{Yb}}^{3/2} \bar{\omega}_{\text{Yb}}^3}{2\pi k_{\text{B}}} \left[ \frac{N_{\text{Cs},\text{single}}}{(T_{\text{Yb}} + \beta_{\text{single}}^{-2} T_{\text{Cs}})^{3/2}} + \frac{N_{\text{Cs},\text{cross}}}{(T_{\text{Yb}} + \beta_{\text{cross}}^{-2} T_{\text{Cs}})^{3/2}} \right]. \end{aligned} \quad (4)$$

Here  $\bar{\omega}_{\text{Yb}} = \sqrt[3]{\omega_x \omega_y \omega_z}$  is the mean Yb trap frequency and  $\beta_j^2$  is defined by  $\beta_j^2 m_{\text{Yb}} \bar{\omega}_{\text{Yb}}^2 = m_{\text{Cs}} \bar{\omega}_{\text{Cs},j}^2$ . Here  $j = \{\text{single}, \text{cross}\}$  denotes the different cases for Cs atoms trapped in the crossed- and single-beam regions.

Due to the large difference in trapping potentials between the two species, Yb experiences a greater gravitational sag than the tightly trapped Cs. For the case of two clouds spatially separated by  $\Delta z$ , the spatial overlap must be reduced by a factor  $F_z(\Delta z)$ , where

$$F_z(\Delta z) = \exp\left(-\frac{m_{\text{Yb}} \omega_{\text{Yb},z}^2 \Delta z^2}{2k_{\text{B}} (T_{\text{Yb}} + \beta_{\text{cross}}^{-2} T_{\text{Cs}})}\right). \quad (5)$$

## III. ANALYSIS OF RESULTS

The coupled equations (1) and (2) are solved numerically. We perform least-squares fits to the experimental results to obtain optimal values of the parameters  $\sigma_{\text{CsYb}}$ ,  $T_{\text{Cs},\text{H}}$  and  $\dot{T}_{\text{Cs},\text{ODT}}$ . The solid lines in Fig. 3 show the results of the fitted model, while the dashed lines show the results in the absence of interspecies collisions. Fig. 3(a) does not include model results, because our analysis does not include the kinetics of Cs atoms entering and leaving the crossed-beam region. We instead constrain the number of Cs atoms inside and outside this region using

interpolating functions (dotted lines in figure) matched to the experimentally measured values.

Since the origin of the heating present on long timescales is unknown, we initially fitted both  $T_{\text{Cs,H}}$  and  $\dot{T}_{\text{Cs,ODT}}$ . We found that these two parameters are strongly correlated, with a correlation coefficient of 0.99 [66]. We therefore choose to extract the parameter  $\dot{T}_{\text{Cs,Heat}}$  corresponding to the total heating rate from both recombination heating and heating due to the ODT. As shown in Fig. 3, the best fit, corresponding to  $\sigma_{\text{Cs}^{174}\text{Yb}} = (5 \pm 2) \times 10^{-13} \text{ cm}^2$  and  $\dot{T}_{\text{Cs,Heat}} = 4 \pm 1 \mu\text{K/s}$ , describes the dynamics of the system well. The large fractional uncertainty in the value of the elastic cross section is primarily due to the large uncertainty in the spatial overlap. We have investigated the effect of systematic errors in the measured parameters of our model and found that the uncertainty in the trap frequency is dominant, and is larger than the statistical error. Inclusion of the correction of (5) is important because the weaker confinement of Yb produces a vertical separation between the two species, reducing the spatial overlap. Initially  $F_z(\Delta z) \sim 0.75$ . Over the timescale of the measurement the spatial overlap reduces further due to the decreasing width of the Cs cloud as it cools. The final value of  $F_z(\Delta z) \sim 0.6$ .

Although the total heating rate is large,  $\dot{T}_{\text{Cs,Heat}} = 4 \pm 1 \mu\text{K/s}$ , it results from the sum of two heating mechanisms, recombination heating and heating from the optical potential. The value for recombination heating is reasonable because the Cs trap depth of  $85 \mu\text{K}$  is large enough to trap some of the products of the three-body recombination event. For our scattering length,  $a_{\text{CsCs}} \approx 250 a_0$ ,  $T_{\text{Cs,H}}$  is still within the range from  $2\epsilon/9$  to  $\epsilon/3$  proposed by the simple model in Ref. [59], where  $\epsilon = \hbar^2/m_{\text{Cs}}(a_{\text{CsCs}} - \bar{a})^2$  with  $\bar{a} = 95.5 a_0$  for Cs. We also cannot rule out any heating effects due to the broadband, multi-mode nature of the trapping laser [62–65] which may inflate the value of  $\dot{T}_{\text{Cs,Heat}}$  above the simple estimate of  $60 \text{ nK/s}$  based upon off-resonant scattering of photons. We find that varying the value of the total trap heating rate  $\dot{T}_{\text{Cs,Heat}}$  over a large range changes the extracted cross section by less than its error.

For the measurements presented in Fig. 3, we deliberately use a low initial density of Cs atoms to avoid three-body recombination collisions dominating the thermalization. This necessitates use of the weakest possible trap and restricts the number of Cs atoms to  $9 \times 10^4$ . However, due to the large ratio of polarizabilities between Cs and Yb (and the effect of gravity), this results in a very shallow trap for Yb. Preparation of Yb atoms in this shallow trap requires that the intraspecies scattering length be favorable for evaporation, currently limiting the Yb isotopes we can study to  $^{170}\text{Yb}$  and  $^{174}\text{Yb}$ . In Fig. 4 we present our thermalization measurements for  $^{170}\text{Yb}$  alongside those for  $^{174}\text{Yb}$ . From the fit to the temperature profile we extract an effective cross section  $\sigma_{\text{Cs}^{170}\text{Yb}} = (18 \pm 8) \times 10^{-13} \text{ cm}^2$  and

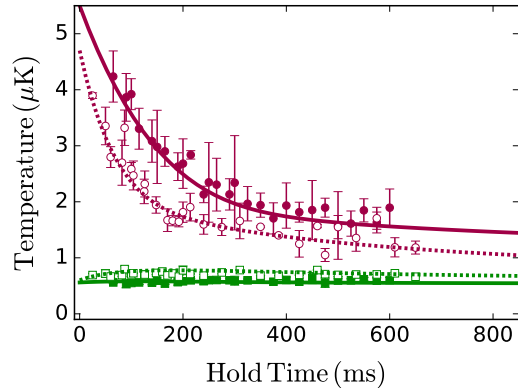


FIG. 4. Thermalization measurements of Cs (red circles) and Yb (green squares) as a function of hold time in the ODT with the other species present. The filled symbols are for  $^{174}\text{Yb}$  as coolant and open symbols are for  $^{170}\text{Yb}$  as coolant. The solid (dotted) lines shows the best fit of our model with  $^{174}\text{Yb}$  ( $^{170}\text{Yb}$ ) as coolant.

$\dot{T}_{\text{Cs,Heat}} = 5 \pm 2 \mu\text{K/s}$ . The larger interspecies cross section allows Cs to be cooled to a lower equilibrium temperature than with  $^{174}\text{Yb}$ . Due to the difference in the natural abundance (31.8% for  $^{174}\text{Yb}$  and 3.0% for  $^{170}\text{Yb}$  [67]) and the intraspecies scattering lengths ( $a_{174} = 105 a_0$  and  $a_{170} = 64 a_0$  [68]), we obtain a number of  $^{170}\text{Yb}$  atoms that is half that of  $^{174}\text{Yb}$ , leading to a greater final temperature for  $^{170}\text{Yb}$ .

#### IV. CALCULATED CROSS SECTIONS AND EXTRACTION OF SCATTERING LENGTHS

Except near narrow Feshbach resonances, CsYb collisions can be treated as those of two structureless particles with an interaction potential  $V(R)$ , which behaves at long range as  $-C_6R^{-6}$ . The scattering length for such a system may be related to  $v_D$ , the non-integer vibrational quantum number at dissociation, by

$$a = \bar{a} \left[ 1 - \tan \left( v_D + \frac{1}{2} \right) \pi \right], \quad (6)$$

where  $\bar{a} = 0.477988 \dots (2\mu C_6/\hbar^2)^{-1/4}$  is the mean scattering length [69] and  $\mu$  is the reduced mass. For CsYb, with  $\sim 70$  bound states [49], changes in the Yb isotope alter  $v_D$  by less than 1, so that the scattering lengths for all possible isotopologs may be placed on a single curve. Determination of the scattering length for one isotopolog allows predictions for all others.

The connection between scattering lengths and effective cross sections for thermalization may be made at various different levels of sophistication. At the lowest temperatures, thermalization is governed by the elastic cross section  $\sigma_{\text{el}} = 4\pi a^2$ . Various energy-dependent corrections to  $\sigma_{\text{el}}$  may be included, from effective-range effects or higher partial waves. However, when higher partial

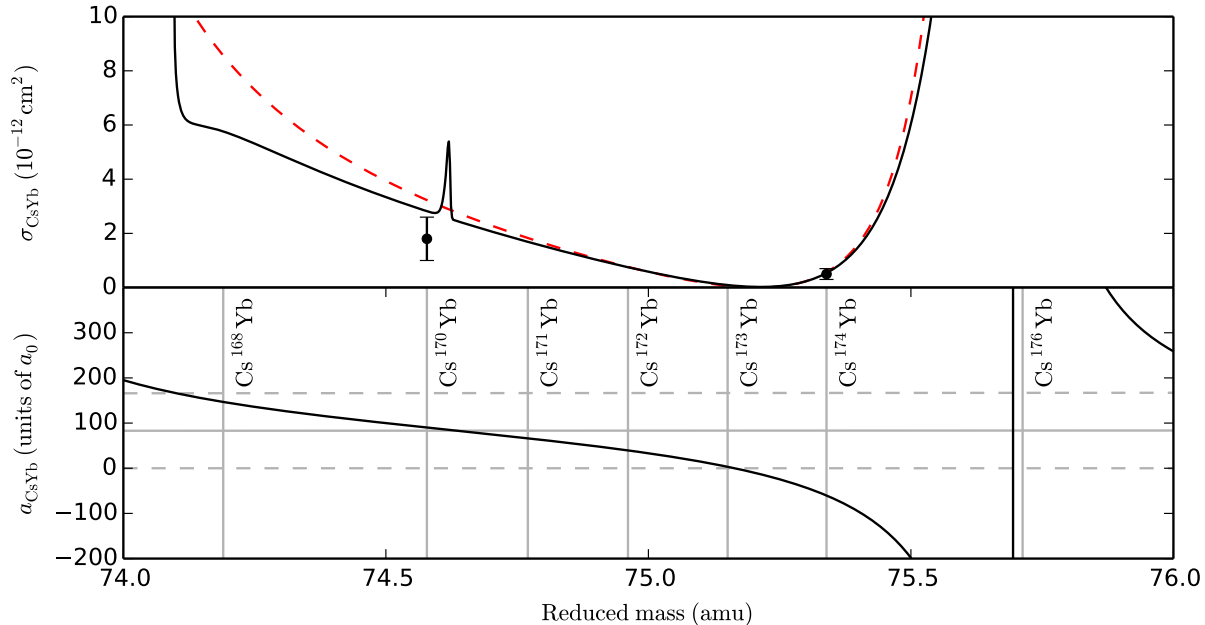


FIG. 5. Top panel: Thermalization cross sections as a function of reduced mass, calculated on potentials optimized using the thermally averaged  $\sigma_\eta^{(1)}$  given by Eq. 7 (black solid line) and the approximation  $\sigma = 4\pi a^2$  (red dashed line). Points show experimentally measured cross sections and error bars correspond to 1 standard deviation. Bottom panel: Calculated scattering length as a function of reduced mass for the potential optimized using  $\sigma_\eta^{(1)}$ . Vertical lines correspond to stable isotopes of Yb. Horizontal lines correspond to 0,  $\bar{a}$  and  $2\bar{a}$ .

waves contribute to the scattering, it is important to replace  $\sigma_{\text{el}}$  with the transport cross section  $\sigma_\eta^{(1)}$ , which accounts for the anisotropy of the differential cross section [70, 71]. p-wave scattering contributes to  $\sigma_\eta^{(1)}$  at considerably lower energy than to  $\sigma_{\text{el}}$ , because of the presence of interference terms between s waves and p waves.

In the present work we calculate  $\sigma_\eta^{(1)}$  explicitly from scattering calculations as described in Ref. [71], using the CsYb interaction potential of Ref. [49]. The resulting energy-dependent cross sections are thermally averaged [70],

$$\sigma_{\text{CsYb}}(T) = \frac{1}{2} \int_0^\infty x^2 \sigma_\eta^{(1)}(x) e^{-x} dx, \quad (7)$$

where  $x = E/k_B T$  is a reduced collision energy. The thermal average is performed at the temperature  $T = \mu(T_{\text{Cs}}/m_{\text{Cs}} + T_{\text{Yb}}/m_{\text{Yb}})$  that characterizes the relative velocity. Note that Eq. 7 contains an extra factor of  $x$  because higher-energy collisions transfer more energy for the same deflection angle.

The scattering length of Eq. 6 depends only on the fractional part of  $\nu_D$ . Small changes in the integer part of  $\nu_D$  have little effect on the quality of fit. We therefore choose to fit the experimental cross sections by varying the interaction potential of Ref. [49] by the minimum amount needed, retaining the number of bound states. We vary the magnitude of its short-range part by a factor

$\lambda$  to vary the scattering length, while keeping the long-range part  $-C_6 R^{-6}$  fixed, with  $C_6$  taken from Ref. [49]. We perform scattering calculations using the MOLSCAT package [72], with the SBE post-processor [73] to evaluate  $\sigma_\eta^{(1)}$  from S-matrix elements.

We obtain optimal values of the potential scaling factor  $\lambda$  by least-squares fitting to the experimental cross sections. The fit using cross sections from Eq. 7 is shown by the solid line in the upper panel of Fig. 5. Also shown (dashed line) is a fit using the approximation  $\sigma = 4\pi a^2$ , with  $a$  obtained from scattering calculations using MOLSCAT. The full treatment of Eq. (7) gives a better fit than the approximation, and it may be seen that there are much larger deviations between the two approaches for other reduced masses. Even though the temperatures of both species are well below the p-wave barrier height of  $\sim 40 \mu\text{K}$ , there is still considerable tunneling through the barrier, which makes important contributions to the thermalization cross sections  $\sigma_\eta^{(1)}$  because of the interference between s-wave and p-wave scattering. The deviations between the approaches are particularly large where  $a$  is close to  $2\bar{a}$ , producing a p-wave shape resonance [74], and there is also a sharp feature where  $a$  is close to  $\bar{a}$ , producing a d-wave shape resonance.

The scattering lengths predicted using the best fitted interaction potential are shown in the lower panel of Fig. 5 for all isotopologs of CsYb. The statistical uncertain-

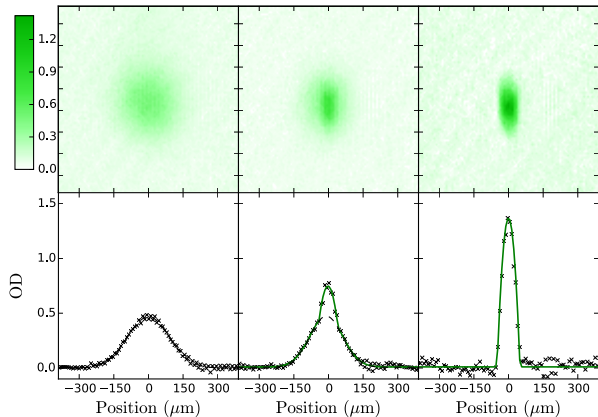


FIG. 6. Bose-Einstein condensation of  $^{174}\text{Yb}$  by evaporative cooling. The top panels show absorption images taken after a 25 ms time of flight. The bottom panels show the corresponding horizontal cross-cuts through the images. The laser power of the optical dipole trap is gradually reduced, cooling the atoms from a thermal cloud at  $T_{\text{Yb}} = 500\text{ nK}$  (left), across the BEC transition to  $T_{\text{Yb}} = 300\text{ nK}$  (middle). Finally, at the end of evaporation a pure condensate (right) is produced containing  $3 \times 10^5$  atoms.

ties in the scattering lengths are quite small,  $a = 90 \pm 2 a_0$  for  $\text{Cs}^{170}\text{Yb}$  and  $-60 \pm 9 a_0$  for  $\text{Cs}^{174}\text{Yb}$ . The fractional error is smaller for  $^{170}\text{Yb}$  than for  $^{174}\text{Yb}$ , because  $\text{Cs}^{170}\text{Yb}$  is in a region of reduced mass  $\mu$  where  $a$  varies only slowly with  $\mu$  and is mostly determined by  $\bar{a}$ , which is accurately known. The systematic uncertainties arising from errors in the number of bound states and the kinetic modeling are harder to quantify, but the qualitative features should nevertheless be reliable. The calculated interspecies scattering lengths are moderately positive for Yb isotopes from 168 to 172, close to zero for 173, and moderately negative for 174. The scattering length for  $\text{Cs}^{176}\text{Yb}$  is predicted to be very large, which may produce relatively broad Feshbach resonances [49].

## V. TOWARDS A DOUBLY DEGENERATE MIXTURE

In our current system, we can independently create Bose-Einstein condensates of Cs and the two Yb isotopes with positive intraspecies scattering lengths and workable abundance,  $^{174}\text{Yb}$  and  $^{170}\text{Yb}$ . The creation of a miscible two-species condensate requires that  $g_{\text{CsYb}}^2 < g_{\text{YbYb}} g_{\text{CsCs}}$ , where the interaction coupling constants are [75]

$$g_{ij} = 2\pi\hbar^2 a_{ij} \left( \frac{m_i + m_j}{m_i m_j} \right). \quad (8)$$

The interspecies scattering lengths obtained above show that both  $\text{Cs}+^{174}\text{Yb}$  and  $\text{Cs}+^{170}\text{Yb}$  BEC mixtures will

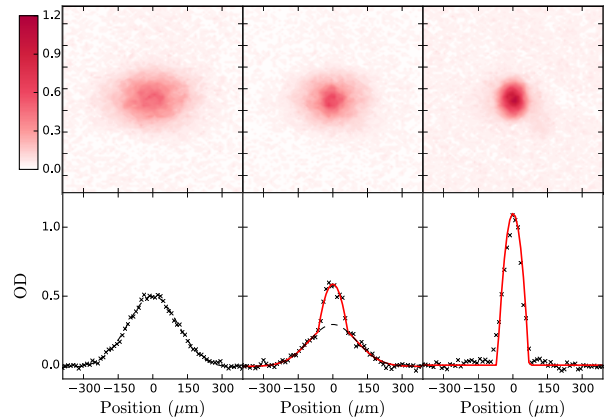


FIG. 7. Bose-Einstein condensation of Cs by evaporative cooling. The top panels show absorption images taken after 50 ms of levitated time of flight. The bottom panels show the corresponding horizontal cross-cuts through the images. The laser power of the optical dipole trap is gradually reduced, cooling the atoms from a thermal cloud at  $T_{\text{Cs}} = 70\text{ nK}$  (left), across the BEC transition to  $T_{\text{Cs}} = 50\text{ nK}$  (middle). Finally, at the end of evaporation a pure condensate (right) is produced containing  $5 \times 10^4$  atoms.

be miscible at the magnetic field required to minimize the Cs three-body loss rate. Moreover, Fig. 5 shows that the interspecies scattering length is predicted to be of moderate magnitude ( $< 200 a_0$ ) for all Yb isotopes except  $^{176}\text{Yb}$ . It should thus also be possible to create stable, miscible quantum-degenerate Cs+Yb mixtures for the less abundant  $^{168}\text{Yb}$  bosonic isotope and the two fermionic isotopes,  $^{171}\text{Yb}$  and  $^{173}\text{Yb}$ . Note that the interspecies scattering length for  $^{172}\text{Yb}$  is large and negative [68], precluding the creation of a large condensate.

The realization of a doubly degenerate mixture will require a trapping arrangement for both species that balances their individual requirements. As a first step, we have created individual BECs of  $^{174}\text{Yb}$  and Cs in the same apparatus. The differing requirements of the two species are highlighted by the different routes we use to create the two condensates. For  $^{174}\text{Yb}$ , the initial steps are the same as in preparing the  $^{174}\text{Yb}$  gas for the thermalization measurements (see Fig. 2), where the sample is loaded into the ODT at high power and evaporatively cooled. However, for BEC the evaporation is continued until the temperature is below the critical temperature,  $T_{c,\text{Yb}} \approx 350\text{ nK}$ , with the power in the ODT ramped down to around 400 mW. Figure 6 shows the transition to BEC for  $^{174}\text{Yb}$ . We typically produce pure  $^{174}\text{Yb}$  BECs containing 3 to  $4 \times 10^5$  atoms.

Preparation of a Cs BEC is a contrasting case. The scattering properties of Cs make the evaporative cooling approach used for  $^{174}\text{Yb}$  impractical. We follow the approach of Ref. [76] and use DRSC to pre-cool a sample of  $5 \times 10^7$  atoms to a temperature  $T_{\text{Cs}} = 2\ \mu\text{K}$ . These atoms are then transferred into a large-volume crossed

Parameter	$^{174}\text{Yb}$	Cs
$U/k_B$ ( $\mu\text{K}$ )	2.5	0.5
$\bar{\omega}/2\pi$ (Hz)	110	45
$P_{\text{Dimple}}$ (mW)	400	3
$T_c$ (nK)	350	60
$N$ ( $T_c$ )	$9 \times 10^5$	$8 \times 10^4$

TABLE I. Parameters for Cs and  $^{174}\text{Yb}$  at the BEC transition.

dipole trap which we call the reservoir trap (see Fig. 1). The reservoir trap is created using a 50 W fiber laser (IPG YLR-50-LP) operating at  $1070 \pm 3$  nm and is formed by two 20 W beams crossing at an angle of  $25^\circ$ , with waists  $440 \pm 10$   $\mu\text{m}$  and  $640 \pm 20$   $\mu\text{m}$ . We initially load  $1.5 \times 10^7$  atoms into the reservoir at  $T_{\text{Cs}} = 2.3$   $\mu\text{K}$ . We then transfer  $9 \times 10^5$  of these atoms into the ODT used previously for thermalization measurements (and for  $^{174}\text{Yb}$  BEC); this is also known as the dimple trap. The bias field is then reduced to 22.3 G to optimize the ratio of elastic to three-body recombination collisions [77] and the sample is evaporatively cooled by reducing the dimple laser power over 2.5 s. The onset of degeneracy occurs at  $T_{\text{c,Cs}} \approx 60$  nK, with the power in the dimple reduced to just 3 mW. The BEC transition for Cs is shown in Fig. 7. We typically obtain pure condensates of 4 to  $5 \times 10^4$  atoms.

Simultaneously creating Cs and Yb BECs in the same optical dipole trap will be very challenging. Table I illustrates that the final trapping powers needed for the independent creation of Cs and Yb BECs are very different. The final trap for  $^{174}\text{Yb}$  requires 400 mW of optical power at 1070 nm, whereas that for Cs requires just 3 mW, even though the trap depths differ by only a factor of 5. The large difference in power stems from the combined effects of the large ratio of the polarizabilities at 1070 nm ( $\alpha_{\text{Cs}}/\alpha_{\text{Yb}} = 7.2$ ) and gravity reducing the depth of the Yb potential. Additionally, the two species require very different traps for efficient evaporative cooling. Cs demands careful management of the three-body loss rate throughout evaporation, requiring more relaxed trapping frequencies and necessitating the use of a reservoir and a dimple trap. By contrast,  $^{174}\text{Yb}$  evaporates most efficiently in a tight trap with large trapping frequencies, due to its much lower three-body loss coefficient [78]. These differences suggest that double degeneracy is unfeasible in the current trapping arrangement.

One solution is to create a tunable optical dipole trap for Cs using a trap wavelength between the Cs  $D_1$  and  $D_2$  lines. In this region the Cs polarizability varies from large positive to large negative values while the Yb polarizability remains almost unchanged. This will allow the ratio of the trap depths (and trap frequencies) to be tuned to a value more favorable for simultaneous cooling of both species. However, due to the relatively low detuning from atomic resonances, photon scattering may become a significant issue for Cs during evaporation. Nevertheless,

such a trap could be used to combine two BECs after independent evaporation.

An alternative approach is the use of a bichromatic trap at 532 nm and 1064 nm. The negative polarizability of Cs at 532 nm ( $\alpha_{\text{Cs}}(532 \text{ nm}) = -210 a_0^3$ ) balances the large positive polarizability at 1070 nm ( $\alpha_{\text{Cs}}(1070 \text{ nm}) = 1140 a_0^3$ ). Because the dominant transition of Yb is at  $\lambda = 399$  nm, Yb is trapped at both wavelengths ( $\alpha_{\text{Yb}}(532 \text{ nm}) = 240 a_0^3$ ,  $\alpha_{\text{Yb}}(1070 \text{ nm}) = 150 a_0^3$ ). Tuning the power of the 532 nm trap lasers thus allows the ratio of trap depths for the two species to be tuned to a suitable value [10, 41].

## VI. CONCLUSIONS

We have measured thermalization in an ultracold mixture of Cs and Yb. We have used a kinetic model to determine the cross sections for interspecies thermalization, taking account of additional heating effects that prevent complete thermalization of the two species. We obtain values of  $\sigma_{\text{Cs}^{174}\text{Yb}} = (5 \pm 2) \times 10^{-13}$   $\text{cm}^2$  and  $\sigma_{\text{Cs}^{170}\text{Yb}} = (18 \pm 8) \times 10^{-13}$   $\text{cm}^2$ . We have carried out quantum scattering calculations of the thermalization cross sections, taking account of anisotropic scattering and thermal averaging, and fitted the short-range part of the CsYb interaction potential to reproduce the experimental results. We have used the resulting interaction potential to calculate scattering lengths for all isotopologs of CsYb.

The interspecies Cs+Yb scattering lengths are predicted to have moderate magnitudes ( $< 200 a_0$ ) for all Yb isotopes except  $^{176}\text{Yb}$ , with good prospects of creating doubly degenerate mixtures. We have cooled both  $^{174}\text{Yb}$  and Cs to degeneracy in the same apparatus, but cooling both species to degeneracy in the same optical trap will be challenging, as illustrated by the contrasting routines we use to produce independent BECs of the two species. We have discussed the use of a tunable-wavelength or bichromatic optical trap that should allow co-trapping of quantum-degenerate Cs+Yb mixtures.

The optimized CsYb potential will assist direct measurements of the CsYb binding energies using two-photon photoassociation spectroscopy [68, 79]. Precise determination of the near-threshold bound states of the molecular potential will allow the accurate prediction and subsequent experimental search for Feshbach resonances that can be used in magnetoassociation to form ultracold  $^2\Sigma$  CsYb molecules.

The data presented in this paper are available online [80].

## ACKNOWLEDGMENTS

We thank I. G. Hughes, M. R. Tarbutt and E. A. Hinds for many valuable discussions. We acknowledge

support from the UK Engineering and Physical Sciences Research Council (Grant Nos. EP/I012044/1 and EP/P01058X/1).

### Appendix: Modeling Thermalization

In order to simulate sympathetic cooling of two distinct atomic species, a simple kinetic model can be used. Here we will derive a system of 4 coupled equations which describe the evolution of the number ( $N_{\text{Cs}}, N_{\text{Yb}}$ ) and temperature ( $T_{\text{Cs}}, T_{\text{Yb}}$ ) of the two species. These can then be solved numerically for given initial conditions and be compared with experimental results (see, for example, Fig. 3). Differentials with respect to time are denoted with a dot above the symbol, for example  $\dot{N}$ . Here we draw together different elements from several similar models [41, 42, 56–60, 81].

We first consider single-species effects, starting with evaporative cooling. If the temperature of the species is not far enough below the trap depth  $U_i$  then atoms with sufficient energy may evaporate from the trap. The dimensionless parameter  $\eta_i = U_i/k_{\text{B}}T_i$  characterizes the trap depth relative to the temperature. Assuming that  $k_{\text{B}}T_i$  is small compared to  $U_i$ , atoms with energy greater than the trap depth are produced at a rate of  $\Gamma_{ii}\eta_i \exp(-\eta_i)$  [58, 81]. The total effective hard-sphere elastic collision rate  $\Gamma_{ii}$  is conveniently written as  $N_i\gamma_{ii}$  where the effective mean collision rate per atom is

$$\gamma_{ii} = \langle n_i \rangle_{\text{sp}} \sigma_{ii} \bar{v}_{ii}, \quad (\text{A.1})$$

where  $\sigma_{ii}$  is the elastic scattering cross-section,  $\bar{v}_{ii} = \sqrt{16k_{\text{B}}T_i/\pi m_i}$  is the mean velocity,  $m_i$  is the mass of species  $i$ , and the mean density is given by

$$\langle n_i \rangle_{\text{sp}} = \frac{N_i}{8} \left( \frac{m_i \bar{\omega}_i^2}{\pi k_{\text{B}} T_i} \right)^{3/2}, \quad (\text{A.2})$$

where  $\bar{\omega}_i = \sqrt[3]{\omega_x \omega_y \omega_z}$  is the mean trap frequency. When an atom evaporates from the trap, it carries away an average energy  $\epsilon_{\text{evap}} = (\eta_i + \kappa_i)k_{\text{B}}T_i$ , where  $\kappa_i = (\eta_i - 5)/(\eta_i - 4)$  [60]; this expression for  $\kappa_i$  is appropriate if  $k_{\text{B}}T_i \ll U_i$  and  $U_i$  is harmonic near the minimum, as is the case in our experiment. The evolution of number and total energy of the ensemble due to evaporation is therefore

$$\dot{N}_{i,\text{evap}} = -N_i \gamma_{ii} \eta_i \exp(-\eta_i), \quad (\text{A.3})$$

$$\dot{E}_{i,\text{evap}} = (\eta_i + \kappa_i)k_{\text{B}}T_i \dot{N}_{i,\text{evap}}. \quad (\text{A.4})$$

The evolution of the temperature can be derived from the relation  $3k_{\text{B}}(T_i \dot{N}_i + \dot{T}_i N_i) = \dot{E}_i$ , to give

$$\dot{T}_{i,\text{evap}} = \eta_i \exp(-\eta_i) \gamma_{ii} \left( 1 - \frac{\eta_i + \kappa_i}{3} \right) T_i. \quad (\text{A.5})$$

If present, inelastic or reactive two-body collisions could also be included in this model. However, since both

Cs and Yb are in their absolute ground state, two-body collisional losses are fully suppressed for our case.

The effect of collisions with background gas is included through the terms

$$\dot{N}_{i,\text{bg}} = -K_{\text{bg}} N_i, \quad (\text{A.6})$$

$$\dot{E}_{i,\text{bg}} = 3k_{\text{B}}T_i \dot{N}_{i,\text{bg}}, \quad (\text{A.7})$$

where  $K_{\text{bg}}$  is the background loss rate, which is taken to be the same for both species. There is no corresponding change in temperature as the loss does not preferentially affect either warmer or cooler atoms.

The inclusion of three-body collisions is essential for this system, due to the large three-body loss coefficient in Cs. The loss rate is given by

$$\dot{N}_{i,3} = -K_{i,3} \langle n_i^2 \rangle_{\text{sp}} N_i, \quad (\text{A.8})$$

where  $\langle n_i^2 \rangle_{\text{sp}} = \sqrt{64/27} \langle n_i \rangle_{\text{sp}}^2$  and  $K_{i,3}$  is the three-body loss coefficient. Because of the density dependence of three-body collisions, atoms are preferentially lost from the high-density region near the center of the trap. The potential energy in this region is lower than the ensemble average, meaning an average excess energy of  $1 k_{\text{B}}T$  remains in the trap for each atom that is lost [59]. In addition to this effect, when three-body recombination produces an atom and a diatom in a state very near threshold, the energy released may be small enough that the atom is not lost, but remains trapped along with a fraction of the energy released [59]. This heating contributes  $k_{\text{B}}T_{i,\text{H}}$  per lost atom. The combination of these two effects gives

$$\dot{E}_{i,3} = (2T_i - T_{i,\text{H}}) k_{\text{B}} \dot{N}_{i,3}, \quad (\text{A.9})$$

$$\dot{T}_{i,3} = K_{i,3} \langle n_i^2 \rangle_{\text{sp}} \frac{T_i + T_{i,\text{H}}}{3}. \quad (\text{A.10})$$

We also introduce an additional term  $\dot{T}_{i,\text{ODT}}$  to account for extra heating from the trapping potential.

We now consider interspecies collisions and the thermalization they cause, as modeling these is our primary purpose. The average energy transfer in a hard-sphere collision is [56]

$$\Delta E_{\text{Cs} \rightarrow \text{Yb}} = \xi k_{\text{B}} \Delta T, \quad (\text{A.11})$$

where  $\Delta T = T_{\text{Cs}} - T_{\text{Yb}}$  and

$$\xi = \frac{4m_{\text{Cs}}m_{\text{Yb}}}{(m_{\text{Cs}} + m_{\text{Yb}})^2} \quad (\text{A.12})$$

reduces the energy transfer for collisions between atoms of different masses. If the collisions are not classical hard-sphere (or purely s-wave) in nature, then different deflection angles  $\Theta$  should be weighted by a factor of  $1 - \cos \Theta$  [70, 71] and the average energy transferred per collision varies from Eq. A.11. Such effects are not included explicitly in this simple kinetic treatment, so the resulting cross sections and collision rates should be interpreted as

effective hard-sphere quantities. We include the effects of deflection angles when we calculate thermalization cross sections from scattering theory in Sec. IV.

In the hard-sphere model, the total energy transferred is just the average energy transferred in a hard-sphere collision multiplied by an effective hard-sphere collision rate  $\Gamma_{\text{CsYb}}$ , giving

$$\dot{E}_{\text{Cs,therm}} = -\xi k_{\text{B}} \Gamma_{\text{CsYb}} \Delta T, \quad (\text{A.13})$$

$$\dot{E}_{\text{Yb,therm}} = +\xi k_{\text{B}} \Gamma_{\text{CsYb}} \Delta T, \quad (\text{A.14})$$

and

$$\dot{T}_{\text{Cs,therm}} = -\frac{\xi \Gamma_{\text{CsYb}} \Delta T}{3N_{\text{Cs}}}, \quad (\text{A.15})$$

$$\dot{T}_{\text{Yb,therm}} = +\frac{\xi \Gamma_{\text{CsYb}} \Delta T}{3N_{\text{Yb}}}. \quad (\text{A.16})$$

Since thermalization collisions do not produce loss,  $\dot{N}_{i,\text{therm}} = 0$ . We can relate the effective rate to an effective cross section  $\sigma_{\text{CsYb}}$  through the relation  $\Gamma_{\text{CsYb}} = \bar{n}_{\text{CsYb}} \sigma_{\text{CsYb}} \bar{v}_{\text{CsYb}}$ . Here,

$$\bar{v}_{\text{CsYb}} = \sqrt{\frac{8k_{\text{B}}}{\pi} \left( \frac{T_{\text{Yb}}}{m_{\text{Yb}}} + \frac{T_{\text{Cs}}}{m_{\text{Cs}}} \right)} \quad (\text{A.17})$$

is the mean collision velocity. The spatial overlap  $\bar{n}_{\text{CsYb}}$  is found by integrating the density distributions of the two species

$$\begin{aligned} \bar{n}_{\text{CsYb}} &= \int [n_{\text{Cs,single}}(\mathbf{r}) + n_{\text{Cs,cross}}(\mathbf{r})] n_{\text{Yb}}(\mathbf{r}) d^3r \\ &= N_{\text{Yb}} \frac{m_{\text{Yb}}^{3/2} \bar{\omega}_{\text{Yb}}^3}{2\pi k_{\text{B}}} \left[ \frac{N_{\text{Cs,single}}}{(T_{\text{Yb}} + \beta_{\text{single}}^{-2} T_{\text{Cs}})^{3/2}} + \frac{N_{\text{Cs,cross}}}{(T_{\text{Yb}} + \beta_{\text{cross}}^{-2} T_{\text{Cs}})^{3/2}} \right], \end{aligned} \quad (\text{A.18})$$

where  $\beta_j^2 = m_{\text{Cs}} \bar{\omega}_{\text{Cs},j}^2 / m_{\text{Yb}} \bar{\omega}_{\text{Yb}}^2$ , where  $j = \{\text{single, cross}\}$  denotes the different cases for Cs atoms trapped in the crossed- and single-beam regions. Eq. A.18 holds true for two clouds centered at the same position, but if the positions of the two clouds are offset in the  $z$  direction by  $\Delta z$  then the spatial overlap must be reduced by a factor

$$F_z(\Delta z) = \exp\left(-\frac{m_{\text{Yb}} \omega_{\text{Yb},z}^2 \Delta z^2}{2k_{\text{B}} (T_{\text{Yb}} + \beta_{\text{cross}}^{-2} T_{\text{Cs}})}\right). \quad (\text{A.19})$$

In our case, the displacement of the clouds is due to gravitational sag and

$$\Delta z = g \left( \frac{1}{\omega_{\text{Cs},z}^2} - \frac{1}{\omega_{\text{Yb},z}^2} \right), \quad (\text{A.20})$$

where  $g$  is the acceleration due to gravity.

Combining all these contributions gives Eqs. 1 and 2.

- 
- [1] G. Modugno, G. Ferrari, G. Roati, R. J. Brecha, A. Simoni, and M. Inguscio, *Science* **294**, 1320 (2001).
- [2] M. Mudrich, S. Kraft, K. Singer, R. Grimm, A. Mosk, and M. Weidemüller, *Phys. Rev. Lett.* **88**, 253001 (2002).
- [3] Z. Hadzibabic, C. A. Stan, K. Dieckmann, S. Gupta, M. W. Zwierlein, A. Görlitz, and W. Ketterle, *Phys. Rev. Lett.* **88**, 160401 (2002).
- [4] M. Taglieber, A.-C. Voigt, T. Aoki, T. W. Hänsch, and K. Dieckmann, *Phys. Rev. Lett.* **100**, 010401 (2008).
- [5] F. M. Spiegelhalter, A. Trenkwalder, D. Naik, G. Hendl, F. Schreck, and R. Grimm, *Phys. Rev. Lett.* **103**, 223203 (2009).
- [6] S. Taie, Y. Takasu, S. Sugawa, R. Yamazaki, T. Tsujimoto, R. Murakami, and Y. Takahashi, *Phys. Rev. Lett.* **105**, 190401 (2010).
- [7] D. J. McCarron, H. W. Cho, D. L. Jenkin, M. P. Köppinger, and S. L. Cornish, *Phys. Rev. A* **84**, 011603 (2011).
- [8] A. Ridinger, S. Chaudhuri, T. Salez, U. Eismann, D. R. Fernandes, K. Magalhães, D. Wilkowski, C. Salomon, and F. Chevy, *The European Physical Journal D* **65**, 223 (2011).
- [9] L. Wacker, N. B. Jørgensen, D. Birkmose, R. Horchani, W. Ertmer, C. Klempt, N. Winter, J. Sherson, and J. J. Arlt, *Phys. Rev. A* **92**, 053602 (2015).
- [10] V. D. Vaidya, J. Tiamsuphat, S. L. Rolston, and J. V. Porto, *Phys. Rev. A* **92**, 043604 (2015).
- [11] M. Gröbner, P. Weinmann, F. Meinert, K. Lauber, E. Kirilov, and H.-C. Nägerl, *Journal of Modern Optics* **63**, 1829 (2016).
- [12] A. S. Flores, H. P. Mishra, W. Vassen, and S. Knoop, *The European Physical Journal D* **71**, 49 (2017).
- [13] S.-K. Tung, K. Jiménez-García, J. Johansen, C. V. Parker, and C. Chin, *Phys. Rev. Lett.* **113**, 240402 (2011).

- (2014).
- [14] R. Pires, J. Ulmanis, S. Häfner, M. Repp, A. Arias, E. D. Kuhnle, and M. Weidemüller, *Phys. Rev. Lett.* **112**, 250404 (2014).
- [15] R. A. W. Maier, M. Eisele, E. Tiemann, and C. Zimmermann, *Phys. Rev. Lett.* **115**, 043201 (2015).
- [16] R. Scelle, T. Rentrop, A. Trautmann, T. Schuster, and M. K. Oberthaler, *Phys. Rev. Lett.* **111**, 070401 (2013).
- [17] J. Catani, G. Barontini, G. Lamporesi, F. Rabatti, G. Thalhammer, F. Minardi, S. Stringari, and M. Inguscio, *Phys. Rev. Lett.* **103**, 140401 (2009).
- [18] T. Köhler, K. Góral, and P. S. Julienne, *Rev. Mod. Phys.* **78**, 1311 (2006).
- [19] K.-K. Ni, S. Ospelkaus, M. De Miranda, A. Pe'er, B. Neyenhuis, J. Zirbel, S. Kotochigova, P. Julienne, D. Jin, and J. Ye, *Science* **322**, 231 (2008).
- [20] F. Lang, K. Winkler, C. Strauss, R. Grimm, and J. H. Denschlag, *Phys. Rev. Lett.* **101**, 133005 (2008).
- [21] K. Aikawa, D. Akamatsu, J. Kobayashi, M. Ueda, T. Kishimoto, and S. Inouye, *New J. Phys.* **11**, 055035 (2009).
- [22] M. P. Köpinger, D. J. McCarron, D. L. Jenkin, P. K. Molony, H.-W. Cho, S. L. Cornish, C. R. Le Sueur, C. L. Blackley, and J. M. Hutson, *Phys. Rev. A* **89**, 033604 (2014).
- [23] P. K. Molony, P. D. Gregory, Z. Ji, B. Lu, M. P. Köpinger, C. R. Le Sueur, C. L. Blackley, J. M. Hutson, and S. L. Cornish, *Phys. Rev. Lett.* **113**, 255301 (2014).
- [24] T. Takekoshi, L. Reichsöllner, A. Schindewolf, J. M. Hutson, C. R. Le Sueur, O. Dulieu, F. Ferlaino, R. Grimm, and H.-C. Nägerl, *Phys. Rev. Lett.* **113**, 205301 (2014).
- [25] J. W. Park, S. A. Will, and M. W. Zwierlein, *Phys. Rev. Lett.* **114**, 205302 (2015).
- [26] M. Guo, B. Zhu, B. Lu, X. Ye, F. Wang, R. Vexiau, N. Bouloufa-Maafa, G. Quémener, O. Dulieu, and D. Wang, *Phys. Rev. Lett.* **116**, 205303 (2016).
- [27] T. A. Isaev, S. Hoekstra, and R. Berger, *Phys. Rev. A* **82**, 052521 (2010).
- [28] V. V. Flambaum and M. G. Kozlov, *Phys. Rev. Lett.* **99**, 150801 (2007).
- [29] J. Hudson, D. Kara, I. Smallman, B. Sauer, M. Tarbutt, and E. Hinds, *Nature* **473**, 493 (2011).
- [30] A. Micheli, G. Pupillo, H. P. Büchler, and P. Zoller, *Phys. Rev. A* **76**, 043604 (2007).
- [31] A. C. Potter, E. Berg, D.-W. Wang, B. I. Halperin, and E. Demler, *Phys. Rev. Lett.* **105**, 220406 (2010).
- [32] K. Góral, L. Santos, and M. Lewenstein, *Phys. Rev. Lett.* **88**, 170406 (2002).
- [33] S. Ospelkaus, K.-K. Ni, D. Wang, M. De Miranda, B. Neyenhuis, G. Quémener, P. Julienne, J. Bohn, D. Jin, and J. Ye, *Science* **327**, 853 (2010).
- [34] R. V. Krems, *Phys. Chem. Chem. Phys.* **10**, 4079 (2008).
- [35] L. Santos, G. V. Shlyapnikov, P. Zoller, and M. Lewenstein, *Phys. Rev. Lett.* **85**, 1791 (2000).
- [36] T. Lahaye, C. Menotti, L. Santos, M. Lewenstein, and T. Pfau, *Reports on Progress in Physics* **72**, 126401 (2009).
- [37] R. Barnett, D. Petrov, M. Lukin, and E. Demler, *Phys. Rev. Lett.* **96**, 190401 (2006).
- [38] A. V. Gorshkov, S. R. Manmana, G. Chen, J. Ye, E. Demler, M. D. Lukin, and A. M. Rey, *Phys. Rev. Lett.* **107**, 115301 (2011).
- [39] B. Yan, S. A. Moses, B. Gadway, J. P. Covey, K. R. A. Hazzard, A. M. Rey, D. S. Jin, and J. Ye, *Nature* **501**, 521 (2013).
- [40] N. Nemitz, F. Baumer, F. Münchow, S. Tassy, and A. Görlitz, *Phys. Rev. A* **79**, 061403 (2009).
- [41] S. Tassy, N. Nemitz, F. Baumer, C. Höhl, A. Batär, and A. Görlitz, *Journal of Physics B: Atomic, Molecular and Optical Physics* **43**, 205309 (2010).
- [42] V. V. Ivanov, A. Khramov, A. H. Hansen, W. H. Dowd, F. Münchow, A. O. Jamison, and S. Gupta, *Phys. Rev. Lett.* **106**, 153201 (2011).
- [43] A. H. Hansen, A. Khramov, W. H. Dowd, A. O. Jamison, V. V. Ivanov, and S. Gupta, *Phys. Rev. A* **84**, 011606 (2011).
- [44] H. Hara, Y. Takasu, Y. Yamaoka, J. M. Doyle, and Y. Takahashi, *Phys. Rev. Lett.* **106**, 205304 (2011).
- [45] F. Baumer, F. Münchow, A. Görlitz, S. E. Maxwell, P. S. Julienne, and E. Tiesinga, *Phys. Rev. A* **83**, 040702 (2011).
- [46] B. Pasquiou, A. Bayerle, S. M. Tzanova, S. Stellmer, J. Szczepkowski, M. Parigger, R. Grimm, and F. Schreck, *Phys. Rev. A* **88**, 023601 (2013).
- [47] A. Micheli, G. Brennen, and P. Zoller, *Nat. Phys.* **2**, 341 (2006).
- [48] P. S. Zuchowski, J. Aldegunde, and J. M. Hutson, *Phys. Rev. Lett.* **105**, 153201 (2010).
- [49] D. A. Brue and J. M. Hutson, *Phys. Rev. A* **87**, 052709 (2013).
- [50] T. Kraemer, M. Mark, P. Waldburger, J. G. Danzl, C. Chin, B. Engeser, A. D. Lange, K. Pilch, A. Jaakkola, H.-C. Nägerl, and R. Grimm, *Nature* **440**, 315 (2006).
- [51] S. L. Kemp, K. L. Butler, R. Freytag, S. A. Hopkins, E. A. Hinds, M. R. Tarbutt, and S. L. Cornish, *Review of Scientific Instruments* **87**, 023105 (2016).
- [52] S. A. Hopkins, K. Butler, A. Guttridge, S. Kemp, R. Freytag, E. A. Hinds, M. R. Tarbutt, and S. L. Cornish, *Review of Scientific Instruments* **87**, 043109 (2016).
- [53] We observe a significant drop in the Cs number when the Cs MOT is operated in the presence of the 399 nm Yb Zeeman slower light. This drop in number is likely due to ionization of Cs atoms in the  $6^2P_{3/2}$  state.
- [54] A. Guttridge, S. A. Hopkins, S. L. Kemp, D. Boddy, R. Freytag, M. P. A. Jones, M. R. Tarbutt, E. A. Hinds, and S. L. Cornish, *Journal of Physics B: Atomic, Molecular and Optical Physics* **49**, 145006 (2016).
- [55] We find that a larger initial density of Cs atoms results in a larger final temperature difference between the two species and a greater loss of Cs atoms during the thermalization.
- [56] A. Mosk, S. Kraft, M. Mudrich, K. Singer, W. Wohlleben, R. Grimm, and M. Weidemüller, *Applied Physics B* **73**, 791 (2001).
- [57] M. Anderlini, D. Ciampini, D. Cossart, E. Courtade, M. Cristiani, C. Sias, O. Morsch, and E. Arimondo, *Phys. Rev. A* **72**, 033408 (2005).
- [58] W. Ketterle and N. V. Druten, *Advances In Atomic, Molecular, and Optical Physics* **37**, 181 (1996).
- [59] T. Weber, J. Herbig, M. Mark, H.-C. Nägerl, and R. Grimm, *Phys. Rev. Lett.* **91**, 123201 (2003).
- [60] K. M. O'Hara, M. E. Gehm, S. R. Granade, and J. E. Thomas, *Phys. Rev. A* **64**, 051403 (2001).
- [61] Estimated to be 60 nK/s for Cs using our trap parameters.
- [62] D. Sofikitis, G. Stern, L. Kime, E. Dimova, A. Fioretti, D. Comparat, and P. Pillet, *The European Physical*

- Journal D **61**, 437 (2011).
- [63] C. R. Menegatti, B. S. Marangoni, N. Bouloufa-Maafa, O. Dulieu, and L. G. Marcassa, *Phys. Rev. A* **87**, 053404 (2013).
- [64] T. Lauber, J. Kber, O. Wille, and G. Birkl, *Physical Review A* **84** (2011), 10.1103/physreva.84.043641.
- [65] K. Yamashita, K. Hanasaki, A. Ando, M. Takahama, and T. Kinoshita, *Physical Review A* **95** (2017), 10.1103/physreva.95.013609.
- [66] I. G. Hughes and T. P. A. Hase, *Measurements and their Uncertainties* (Oxford University Press, 2010).
- [67] J. R. De Laeter, J. K. Böhlke, P. De Bièvre, H. Hidaka, H. S. Peiser, K. J. R. Rosman, and P. D. P. Taylor, *Pure and Applied Chemistry, Pure Appl. Chem.* **75**, 683 (2009).
- [68] M. Kitagawa, K. Enomoto, K. Kasa, Y. Takahashi, R. Ciuryło, P. Naidon, and P. S. Julienne, *Phys. Rev. A* **77**, 012719 (2008).
- [69] G. F. Gribakin and V. V. Flambaum, *Phys. Rev. A* **48**, 546 (1993).
- [70] M. Anderlini and D. Guéry-Odelin, *Phys. Rev. A* **73**, 032706 (2006).
- [71] M. D. Frye and J. M. Hutson, *Phys. Rev. A* **89**, 052705 (2014).
- [72] J. M. Hutson and S. Green, “MOLSCAT computer program,” (2011).
- [73] J. M. Hutson and S. Green, “SBE computer program,” distributed by Collaborative Computational Project No. 6 of the UK Engineering and Physical Sciences Research Council (1982).
- [74] B. Gao, *Phys. Rev. A* **62**, 050702 (2000).
- [75] F. Riboli and M. Modugno, *Phys. Rev. A* **65**, 063614 (2002).
- [76] T. Kraemer, J. Herbig, M. Mark, T. Weber, C. Chin, H.-C. Nägerl, and R. Grimm, *Applied Physics B* **79**, 1013 (2004).
- [77] T. Weber, J. Herbig, M. Mark, H.-C. Nägerl, and R. Grimm, *Science* **299**, 232 (2003).
- [78] Y. Takasu, K. Maki, K. Komori, T. Takano, K. Honda, M. Kumakura, T. Yabuzaki, and Y. Takahashi, *Phys. Rev. Lett.* **91**, 040404 (2003).
- [79] F. Munchow, C. Bruni, M. Madalinski, and A. Gorlitz, *Phys. Chem. Chem. Phys.* **13**, 18734 (2011).
- [80] Durham University Collections, <http://dx.doi.org/10.15128/r2rv042t06m>.
- [81] O. J. Luiten, M. W. Reynolds, and J. T. M. Walraven, *Phys. Rev. A* **53**, 381 (1996).